Decisive role of nonlinear temperature advection in El Niño and La Niña amplitude asymmetry

Wansuo Duan,[1] Hui Xu,[1] and Mu Mu[1]

Received 16 October 2006; revised 15 August 2007; accepted 24 October 2007; published 19 January 2008.

[1] The asymmetry of El Niño and La Niña in amplitude is a distinct feature of the observed El Niño–Southern Oscillation (ENSO). In this paper, we investigate the theoretical ENSO asymmetry by applying conditional nonlinear optimal perturbation in a theoretical model and an intermediate ENSO model. It is shown that the nonlinear temperature advection (NTA) plays an important role in ENSO asymmetry. By investigating the different types of nonlinearities in the Zebiak-Cane model, we identify clearly the origin of ENSO asymmetry and further emphasize the decisive role of the NTA. The NTA enhances the El Niño amplitude but has little effect on La Niña, resulting in the asymmetry of ENSO in amplitude. We also demonstrate that the stronger the El Niño event is, the larger the nonlinear effect related to the NTA is and the more significant the ENSO asymmetry is. This finding may explain why the strong ENSO events after the 1976 climate shift are of significant asymmetry.

Citation: Duan, W., H. Xu, and M. Mu (2008), Decisive role of nonlinear temperature advection in El Niño and La Niña amplitude asymmetry, *J. Geophys. Res.*, *113*, C01014, doi:10.1029/2006JC003974.

1. Introduction

[2] The complexity of the ocean-atmosphere interactions poses great difficulties for theoreticians to explain El Niño–Southern Oscillation (ENSO) using simple models. The linear dynamics of ENSO provided essential insights into the mechanisms responsible for the periodicity of ENSO [*Philander*, 1983; *Jin*, 1997a, 1997b; *Wang*, 2001], but it cannot explain what governs its amplitude.

[3] The amplitude of the observed El Niño is larger than that of La Niña, which is a distinct feature of ENSO and is referred to as ENSO asymmetry in literatures [*Jin et al.*, 2003; *An and Jin*, 2004; *Duan et al.*, 2004]. Furthermore, there is evidence that ENSO asymmetry has become pronounced since the climate shift around the year 1976, from a relatively stable to an unstable oscillating system [*An and Jin*, 2000; *Wang and An*, 2001; *Duan and Mu*, 2006]. Before 1976, the amplitudes of El Niño were moderate; after 1976, they are much large, with intensities up to about 4.0°C in terms of Niño-3 index, compared to −2.0°C for La Niña.

[4] ENSO asymmetry needs to be addressed in terms of a dynamical regime in which ENSO operates. Hypotheses for ENSO can be loosely grouped into three types. First, El Niño is one phase of a self-sustained, unstable, and naturally oscillatory mode of the coupled ocean-atmosphere system [*Zebiak and Cane*, 1987; *Münnich et al.*, 1991; *Timmermann and Jin*, 2002]. In this scenario, nonlinearity plays an important role in controlling ENSO amplitude [*Jin*, 1997a, 1997b]. Second, El Niño is a stable (or damped) mode triggered by atmospheric random "noises" [*Peland and Sardeshmukh*, 1995]. Third, it is also possible that El Niño is a self-sustained mode during some periods, a stable mode during others, or a mixed mode of the two (see the review of *Wang and Picaut* [2004]).

[5] Attention has been paid to the study of ENSO asymmetry. *An and Jin* [2004], *Rodgers et al.* [2004], and *Duan et al.* [2004] demonstrated that ENSO asymmetry is a typical nonlinear property of a coupled ocean-atmosphere system [see also *Jin et al.*, 2003]. *An and Jin* [2004] examined the dynamical role of the nonlinear heating in ENSO asymmetry. In this paper, we will use a new approach of conditional nonlinear optimal perturbation (CNOP) to investigate the roles of different types of nonlinearities in ENSO asymmetry and show the decisive role of nonlinear temperature advection (NTA). Furthermore, we will provide a possible mechanism responsible for the effect of the NTA on ENSO asymmetry.

2. Conditional Nonlinear Optimal Perturbation

[6] The CNOP is an initial perturbation that satisfies a given constraint and has the largest nonlinear evolution at prediction time [*Mu et al.*, 2003]. This approach has been used to study the dynamics of ENSO predictability [*Mu and Duan*, 2003; *Duan et al.*, 2004; *Duan and Mu*, 2006] and the sensitivity of ocean thermohaline circulation (THC) [*Mu et al.*, 2004], as well as the passive variability of THC [*Sun et al.*, 2005]. These studies have shown that CNOP is one of the useful tools to reveal the effect of nonlinearity on climate predictability. For readers' convenience, we briefly review the CNOP approach as follows.

[7] Let M_τ be the propagator of a nonlinear model, which "propagates" the initial value to the future time τ. Here u_0 is an initial perturbation superposed on a basic state $U(t)$, which

[1]State Key Laboratory of Numerical Modeling for Atmospheric Sciences and Geophysical Fluid Dynamics (LASG), Institute of Atmospheric Physics, Chinese Academy of Sciences, Beijing, China.

0148-0227/08/2006JC003974

is a solution to the nonlinear model and satisfies $U(\tau) = M_\tau(U_0)$ at time τ (U_0 is the initial value of $U(t)$).

[8] For a chosen norm $\|\cdot\|$, an initial perturbation $u_{0\delta}$ is called CNOP, if and only if

$$J(u_{0\delta}) = \max_{\|u_0\| \le \delta} \| M_\tau(U_0 + u_0) - M_\tau(U_0) \|,$$

where $\|u_0\| \le \delta$ is a constraint for initial perturbations defined by norm.

[9] CNOP is the global maximum of J. There exists possibility that the objective function J attains its local maximum in a small neighborhood of a point in the phase space. Such initial perturbation is called local CNOP [*Mu and Zhang*, 2006].

[10] Both CNOP and local CNOP possess clear physical meanings [*Mu and Duan*, 2005]. *Duan et al.* [2004] demonstrated that when the objective function measures the maximum evolution of sea surface temperature anomaly (SSTA) for ENSO, the obtained CNOP (local CNOP) superimposed on the climatological basic state acts as the initial anomaly mode that is most likely to evolve into El Niño (La Niña) event and represents the optimal precursor of El Niño (La Niña). For the initial anomalies satisfying the given constraint, the El Niño event caused by CNOP is the strongest one. From the viewpoint of signal-to-noise rate, the optimal precursor of El Niño in ENSO model can be considered the most predictable mode, meaning that if this signal is observed in nature then the future outcome of the system is fairly certain. *Clarke and van Gorder* [1999] demonstrated that some observed ENSO events after 1976 climate shift are strong signal and therefore of relatively strong predictability, such as the 1982/1983 and 1997/1998 El Niño events. Since the ENSO events caused by CNOPs have similar properties to those of strong ENSO events in observation, we will use CNOP approach to explore the asymmetry of strong ENSO events mentioned in the introduction.

[11] CNOP and local CNOP can be computed by using Spectral Projected Gradient 2 (SPG2) algorithm, which is used to solve nonlinear minimization problems with equality and/or inequality constraint condition. Detailed description is given by *Birgin et al.* [2000].

3. Results

[12] To investigate the asymmetry of ENSO, we first perform some numerical experiments to the simple ENSO model of *Wang and Fang* [1996] (hereinafter WF96) and then the intermediate model developed by *Zebiak and Cane* [1987] (hereafter referred to as ZC model). On the basis of these two models of varying complexity, a unified explanation to the ENSO asymmetry is presented.

3.1. Theoretical Model Results

[13] The theoretical WF96 model consists of two dimensionless prognostic equations for SSTA, T, and thermocline depth anomaly, h, in Niño-3 region as follows.

$$\begin{cases} \frac{dT}{dt} = a_1 T - a_2 h + \sqrt{\frac{2}{3}} T(T - \gamma h), \\ \frac{dh}{dt} = b(2h - T), \end{cases} \quad (1)$$

Table 1. Values of the Model Parameters

Parameter	Value
α	0.0225
μ	1.315
δ_1	0.0848
α_s	$(125\ \text{days})^{-1}$
H	150 m
H_1	50 m
L_0	300 km
L_s	338 km

where $a_1 = \bar{T}_z + \bar{T}_x - \alpha_s$, $a_2 = \mu\bar{T}_x$, $b = (2\alpha)/(p(1 - 3\alpha^2))$, $\gamma = \mu + \delta_1$, and $p = (1 - H_1/H)(L_0/L_s)^2$. The characteristic scales of SSTA and thermocline depth anomaly are 2.0°C and 50 m (WF96), respectively. The expressions $\bar{T}_z T$, $\bar{T}_x(T - \mu h)$, and $-\alpha_s T$ are linear terms in the temperature equation that come from the vertical advection by the anomalous upwelling of the mean ocean temperature ($w\bar{T}_z$), the vertical advection by the mean upwelling of the anomalous ocean temperature ($\bar{w}T_z$), and the linear damping. The coefficients a_1 and a_2 involve basic state parameters $\bar{T}_x$ and $\bar{T}_z$, which characterize, respectively, the mean temperature difference between the equatorial eastern and western basins and between the mixed-layer and subsurface-layer water. These basic state parameters can be time-dependent, reflecting the climatological annual cycle of the basic state. The quadratic term in temperature equation is deduced from the NTA by anomalous upwelling of the anomalous temperature (see section 4.2). The linear terms in h-Eq depict the effect of equatorial waves on thermocline adjustment ($2bh$) and the effect of the wind forcing ($-bT$). Some nondimensional coupling parameters are presented in this model (WF96): α is the air-sea coupling coefficient, μ measures the degree of coupling between thermocline fluctuation and SST, and δ_1 represents the contribution of the horizontal temperature advection by anomalous zonal currents to local SST variation. There are also some basic parameters in the WF96 model: the Newtonian cooling coefficient α_s, the mean depth of the thermocline H, and the depth of the mixed layer H_1, the oceanic Rossby radius of deformation L_0, and the Ekman spreading length scale L_s. The typical values of these parameters are listed in Table 1 (WF96).

[14] Let $\boldsymbol{u}_0$ be an initial anomaly. A nonlinear optimization problem related to CNOP is then defined as follows.

$$J(\boldsymbol{u}_{0\delta}) = \max_{\|\boldsymbol{u}_0\| \le \delta} |T(\tau)|, \quad (2)$$

where $T(\tau)$ is the evolution of model SSTA obtained by integrating the WF96 model from 0 to τ with an initial value u_0. Thus $J(\boldsymbol{u}_{0\delta})$ describes the maximum evolution of SSTA at prediction time τ. By solving this optimization problem, the optimal initial perturbations satisfying the constraint $\|\boldsymbol{u}_0\| \le \delta$, i.e., CNOPs, $\boldsymbol{u}_{0\delta}$, can be found. As mentioned above, these CNOPs represent the optimal precursors for ENSO.

[15] We choose the norm $\|\boldsymbol{u}_0\| = \sqrt{T_0^2 + h_0^2}$ to define the constraint condition [*Duan et al.*, 2004], where T_0 and h_0 are the initial values of nondimensional SSTA and thermocline depth anomaly. Then the optimization problem (equation (1)) is solved for the time interval τ = 12 months

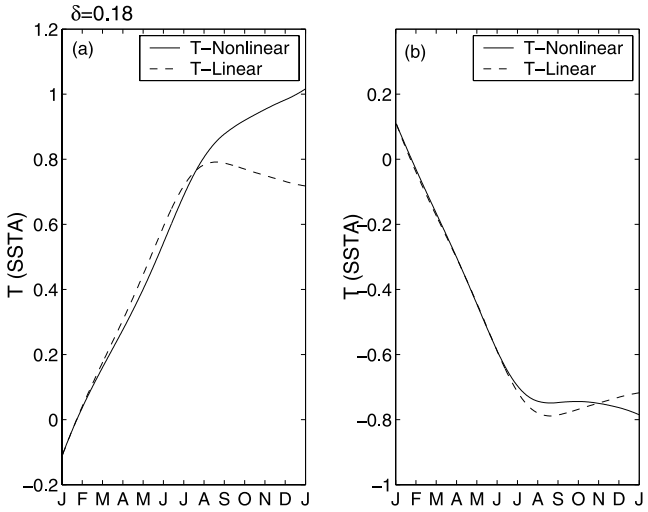

Figure 1. SSTA components (Nino-3 index) of nonlinear (solid line) and linear (dashed line) evolutions of CNOP and local CNOP with $\delta = 0.18$ in the WF96 model. (a) For CNOP and (b) for local CNOP.

with initial time as January. It is shown that there exist a CNOP and a local CNOP of the annual cycle for the constraint $\|\boldsymbol{u}_0\| \leq \delta$ with $\delta \in [0.05, 0.25]$. For $\delta = 0.18$, the CNOP and local CNOP are $(-0.1130, 0.1401)$ and $(0.1141, -0.1390)$, respectively; for $\delta = 0.20$, they are $(-0.1208, 0.1594)$ and $(0.1259, -0.1554)$. These CNOPs and local CNOPs locate the boundary of the constraint disk and the values of δ indicate the magnitude of them. Furthermore, they are, respectively, most likely to evolve into El Niño and La Niña events and acts as the optimal precursors of El Niño and La Niña [*Duan et al.*, 2004; *Duan and Mu*, 2006]. In the following, we will use these model ENSO events with CNOPs (local CNOPs) in January to investigate ENSO asymmetry.

[16] Integrating the WF96 model with initial anomalies that are CNOPs and local CNOPs of different magnitudes, we obtain their nonlinear evolutions. In Figures 1a and 2a, we plot the SSTA evolutions of CNOP with $\delta = 0.18$ and 0.20, respectively. It is shown that these CNOPs develop into El Niño events with different intensities. The larger the CNOP measured by norm is, the stronger the corresponding El Niño event is. The behaviors of local CNOP with $\delta = 0.18$ and $\delta = 0.20$ are respectively illustrated in Figures 1b and 2b, which correspond to two La Niña events with different intensities.

[17] To explore the effect of nonlinearity on ENSO amplitude, we also investigate the evolutions of both CNOP and local CNOP in the tangent linear model (TLM) of the WF96 model, which is obtained by linearizing the nonlinear term $\eta(T, h) = T(T - \gamma h)$. The evolutions of CNOP and local CNOP in the TLM are also an El Niño and a La Niña events, which are plotted in Figures 1 and 2.

[18] The comparisons are performed between the nonlinear behavior of CNOP and that of local CNOP, and between their linear evolutions. The results demonstrate that for a given value of δ, the El Niño events caused by CNOP are considerably stronger than the La Niña caused by local CNOP (see Figures 1 and 2). Therefore they are asymmetric in amplitude, which agrees qualitatively with the observed ENSO asymmetry. On the other hand, we notice that the El Niño and La Niña events in TLM have very similar amplitudes for a given value of δ. For example, for $\delta = 0.20$ the peak value of the El Niño (La Niña) events in TLM is about 0.9 (-0.9; nondimensionalized), or 1.8°C (-1.8°C; see Figure 2). From these results, we can clearly see that nonlinearity plays an important role in ENSO asymmetry. Then, how does the nonlinearity cause ENSO asymmetry?

[19] From Figures 1a and 2a, it is seen that the El Niño events in the WF96 model are notably stronger than those in the TLM for the same CNOP-type initial anomaly. However, the La Niña events in the WF96 model and its TLM with the same local CNOP as initial anomaly remain only trivially different (see Figures 1b and 2b). It is therefore very clear that nonlinearity enhances El Niño and negligibly affects La Niña, leading to the asymmetry of ENSO. Furthermore, Figures 1 and 2 show that this kind of asymmetry has clear seasonality. In fact, the largest asymmetry occurs during the mature phase (i.e., winter) of an El Niño event. In addition, it is also clear from Figure 3 that the larger the CNOPs as measured by the chosen norm, the more significant the differences between the El Niño events in the WF96 model and in its TLM (Figure 3). That is to say, the larger the CNOP is, the more asymmetric the ENSO asymmetry is.

[20] The norm $\|\boldsymbol{u}_0\|_2 = \max\{|T_0|, |h_0|\}$ is also adopted to define the constraint of initial anomalies. The CNOP and local CNOP satisfying the constraint $\|\boldsymbol{u}_0\|_2 \leq \delta$ are also solved. Furthermore, we have conducted a large number of numerical experiments and obtained similar results to those shown by norm $\|\cdot\|$. For simplicity, the details are not given here.

[21] The numerical results show the effect of nonlinearity on ENSO asymmetry. The nonlinear term in WF96 only enhances El Niño amplitude, not La Niña, resulting in ENSO asymmetry. Section 3 pointed out that the nonlinear term in the WF96 model comes from the NTA. However, the WF96 model is a highly simplified one; its nonlinearity only includes the anomalous temperature advection. Furthermore, the robustness of the results needs to be established in more realistic models. Next, we will use the ZC

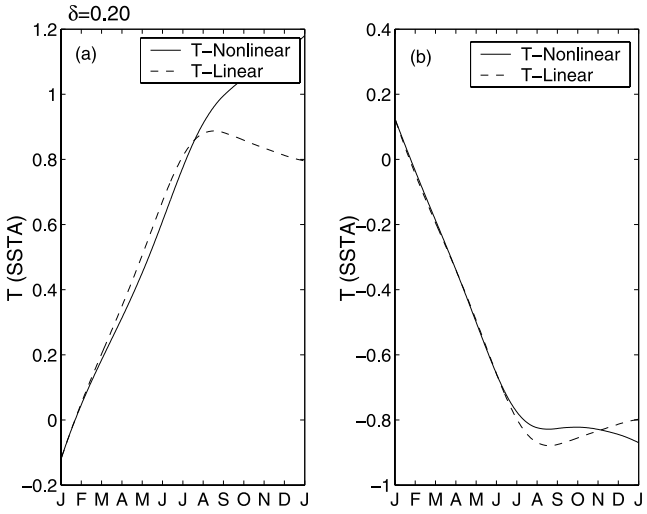

Figure 2. Same as Figure 1 except for $\delta = 0.20$.

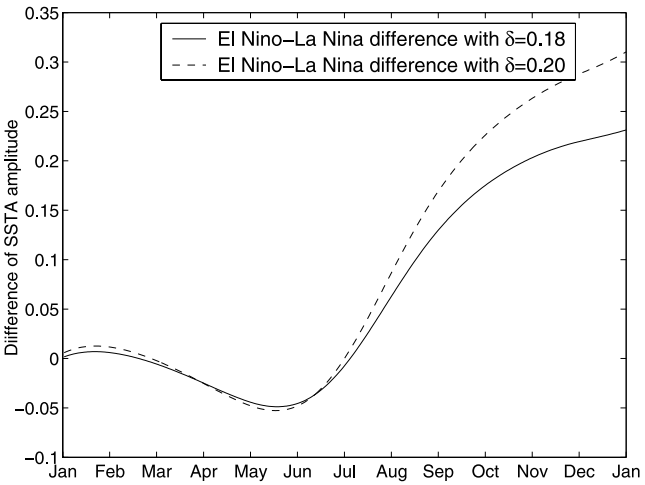

Figure 3. Amplitude difference between El Niño and La Niña in the WF96 model, where the amplitude is measured by the absolute value of SSTA (Nino-3 index). The solid (dashed) line denotes the case of $\delta = 0.18$ ($\delta = 0.20$), which is obtained by subtracting the absolute value of SSTA for La Niña from that for El Niño.

model to investigate the role of the NTA in ENSO asymmetry by CNOP approach and to verify the results of the WF96 model.

3.2. Intermediate Model Results

[22] The temperature equation of the ZC model is

$$\frac{\partial \boldsymbol{T}}{\partial t} = -\bar{\boldsymbol{U}} \cdot \nabla \boldsymbol{T} - \boldsymbol{U} \cdot \nabla(\bar{\boldsymbol{T}} + \boldsymbol{T}) - \{M(\bar{\boldsymbol{w}}_s + \boldsymbol{w}_s) - M(\bar{\boldsymbol{w}}_s)\} \times \bar{\boldsymbol{T}}_z - M(\bar{\boldsymbol{w}}_s + \boldsymbol{w}_s)\boldsymbol{T}_z - \alpha_s T, \quad (3)$$

where T, $\boldsymbol{U}$, $\boldsymbol{w}_s$, and $\bar{\boldsymbol{w}}_s$ denote anomalies of mixed layer temperature (or SST), horizontal surface velocity (a vector), the upwelling at the mixed layer base, and the mean upwelling. The coefficient α_s is a nondimensional parameter that represents the Newtonian cooling coefficient for SSTA. The function $M(x)$ is defined by

$$M(x) = \begin{cases} 0, x \le 0, \\ x, x > 0. \end{cases} \quad (4)$$

It accounts for the fact that surface temperature is affected by vertical advection only in the presence of upwelling. The anomalous vertical temperature gradient, T_z, is defined by

$$\boldsymbol{T}_z = \frac{\boldsymbol{T} - \boldsymbol{T}_e}{H_1}, \quad (5)$$

where H_1 is the surface layer thickness, and T_e measures the temperature anomalies entrained into the surface layer.

[23] To investigate ENSO asymmetry, we construct a cost function to measure the evolution of initial anomalies, which is similar to that in section 3.1. Then the optimal precursor of El Niño (La Niña), CNOP (local CNOP), can be obtained by solving

$$J(\boldsymbol{u}_{0\delta}) = \max_{\|\boldsymbol{u}_0\|_a \le \delta} \|\boldsymbol{T}(\tau)\|_b, \quad (6)$$

where $\boldsymbol{u}_0 = (w_1^{-1}\boldsymbol{T}_0, w_2^{-1}\boldsymbol{h}_0)$ is the nondimensional initial SSTA and thermocline depth anomaly, w_1 and w_2 denote the characteristic scales of dimensional SSTA and thermocline depth anomaly and are taken as those of the WF96 model, i.e., $w_1 = 2.0°C$ and $w_2 = 50$ m. The condition $\|\boldsymbol{u}_0\|_a \le \delta$ is the constraint defined by the norm $\|\boldsymbol{u}_0\|_a = \sqrt{\sum_{i,j}\left\{\left(w_1^{-1}T_{0i,j}\right)^2 + \left(w_2^{-1}h_{0i,j}\right)^2\right\}}$, where (i, j) represents a grid point in the region from 129.375E to 84.375W by grid spacing 5.625 degrees and from 19S to 19N by grid spacing 2 degrees. Variables $T_{0i,j}$ and $h_{0i,j}$ denote the dimensional SST and thermocline depth anomalies at grid point (i, j). The evolutions of these initial anomalies are measured by the norm $\|\boldsymbol{T}(\tau)\|_b = \sqrt{\sum_{i,j}\left(w_1^{-1}T_{i,j}(\tau)\right)^2}$, and $T_{i,j}(\tau)$ is obtained by integrating the ZC model from time 0 to τ with a proper initial condition $\boldsymbol{u}_0$.

[24] For $\delta \in [0.6, 1.2]$, the optimal perturbations satisfying the condition $\|\boldsymbol{u}_0\|_a \le \delta$, i.e., CNOPs, are obtained, which are most likely to evolve into El Niño events in the ZC model. There also exist local CNOPs that are most likely to develop into La Niña events. Furthermore, for the same magnitude of initial anomalies, the El Niño events caused by CNOPs are significantly stronger than the La Niña events caused by local CNOPs. The corresponding statistical significance is determined as follows.

[25] The Wilcoxon signed-rank method [*Wilcoxon*, 1945] can be used to test the significance for the difference of the mean of two sets of samples. We denote these two samples as x_i^E and x_i^L, where $i = 1, 2, 3\ldots, n$. Let $y_i = x_i^E - x_i^L$. We sort by size the absolute values of y_i as $z_{(1)} < z_{(2)} < \cdots < z_{(n)}$. If $|y_i| = z_{(Ri)}$, the rank of $|y_i|$ is R_i, where $R_i = 1, 2, 3, \cdots, n$. The Wilcoxon signed ranked statistic is determined by

$$W^+ = \sum_{i=1}^{n} = u_i R_i,$$

where

$$u_i = \begin{cases} 1, & y_i > 0, \\ 0, & \text{otherwise.} \end{cases}$$

In our case, we take the peak values of El Niño (La Niña) events caused by CNOPs (local CNOPs) as the ensemble members. These CNOPs (local CNOPs) are for the time interval $\tau = 12$ months with the initial times January, March, May, July, September, and November, where the initial constraints are chosen as $\|u_0\|_a \le 0.8$ and $\|u_0\| \le 1.0$, respectively. Integrating the ZC model with these CNOPs and local CNOPs as initial values, we obtain 12 pairs of El Niño and La Niña events. Then the absolute of the peak values for these El Niño and La Niña events form two independent sets, x_i^E and x_i^L, with the sample size as $m_1 = m_2 = 12$. By using x_i^E and x_i^L, we get $W^+ = 231$. The corresponding probability $p = 2P(W^+ \ge 231)$. The critical values of $n = m_1 + m_2 = 24$ at significance level 5% is $n = 209$. Thus we have $p < 2P(W^+ \ge 209) = 0.05$. This indicates that the El Niño events in the ZC model are significantly stronger than the La Niña events. Therefore they are significantly asymmetric in terms of amplitudes.

[26] Now let us investigate the dynamics of ENSO asymmetry in the ZC model by the above CNOPs and local

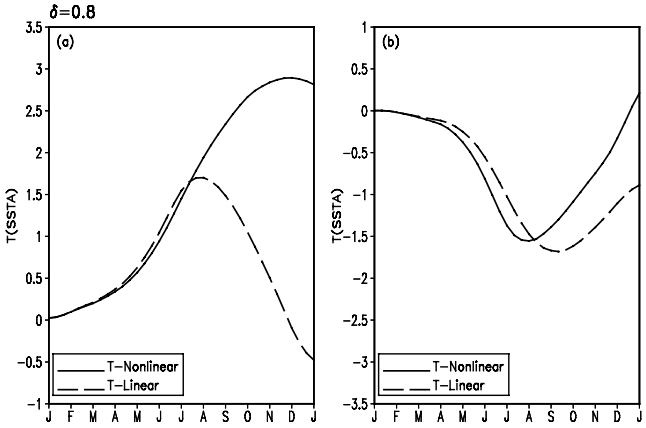

Figure 4. SSTA components of the evolutions of CNOP (local CNOP) for $\delta = 0.8$ in the full (solid line) and PL-ZC (dashed line) models. (a) For CNOP and (b) for local CNOP.

CNOPs. In particular, we take the CNOPs and local CNOPs with initial time as January for both $\delta = 0.8$ and $\delta = 1.0$ as examples to describe the results. Figures 4 and 5 demonstrate that the CNOPs (local CNOPs) for $\delta = 0.8$ and 1.0 evolve into El Niño (La Niña) events, with the event strength increasing with δ. For $\delta = 0.8$, the El Niño event has a peak SSTA value of 2.8°C (Niño-3 index), while the La Niña event has the peak value of −1.6°C. For $\delta = 1.0$, the peak value for El Niño in is about 3.4°C, and that for La Niña is about −1.8°C. As a result, the amplitude difference is about 1.6°C, while for $\delta = 0.8$ it is about 1.2°C. It is obvious that the stronger the El Niño events caused by CNOP is, the larger the asymmetry of El Niño and La Niña is. This result agrees qualitatively with that of the WF96 model.

[27] The results of the WF96 model have shown that the asymmetry of ENSO is formalized by the NTA enhancing aggressively El Niño and negligibly affecting La Niña amplitude. To test whether or not this result is true in the ZC model, we rewrite equation (3) as

$$\frac{\partial \boldsymbol{T}}{\partial t} = -\bar{\boldsymbol{U}} \cdot \nabla \boldsymbol{T} - \boldsymbol{U} \cdot \nabla \bar{\boldsymbol{T}} - \{M(\bar{\boldsymbol{w}}_s + \boldsymbol{w}_s) - M(\bar{\boldsymbol{w}}_s)\} \times \bar{\boldsymbol{T}}_z - M(\bar{\boldsymbol{w}}_s)\boldsymbol{T}_z + \psi(U, w_s) - \alpha_s T,$$

where $\psi(U, w_s) = \boldsymbol{U} \cdot \nabla \boldsymbol{T} - (M(\bar{\boldsymbol{w}}_s + \boldsymbol{w}_s) - M(\bar{\boldsymbol{w}}_s))\boldsymbol{T}_z$ is a nonlinear term that represents the anomalous temperature advection, the NTA term. After linearizing this term, we obtain a partially linearized ZC model (hereinafter referred to as PL-ZC model) and integrate it with the above CNOPs and local CNOPs as initial values. Two time series of SSTA are obtained (Figures 4 and 5). Note that these two time series correspond to an El Niño and a La Niña events, respectively. They have almost the same amplitude; for example, the maximum amplitude of SSTA for $\delta = 0.8$ is about 1.7°C. That is, they are nearly symmetric in the PL-ZC model. However, as demonstrated above, the resultant El Niño and La Niña by the full ZC model are asymmetric in amplitude. Therefore we confirm that the NTA plays an important role in the asymmetry of El Niño and La Niña. Furthermore, Figures 4 and 5 show that the El Niño events in the full ZC model are considerably stronger than those in the PL-ZC model, while the La Niña events in these two models remain trivially different in amplitude. These results of the ZC model support qualitatively those of the theoretical WF96 model.

[28] The ZC model has several nonlinear terms including the parameterization of subsurface temperature, the anomalous temperature advection (i.e., the NTA term), and the anomalous wind stress. In the above, we have examined the role of anomalous temperature advection. With the NTA term, the El Niño and La Niña in the ZC model are asymmetric, without it the El Niño and La Niña in the PL-ZC model are symmetric. This indicates that the NTA determines the ENSO asymmetry and plays a decisive role. To further test this idea, we performed the following two groups of sensitivity experiments.

[29] In the first group of experiments, the wind stress anomaly term of the ZC model was linearized while the other nonlinear terms remained unchanged. During an El Niño event, the nonlinear wind stress anomaly tends to be positive, namely, a westerly anomaly. However, the linearized wind stress anomaly has a much large magnitude compared to that in the nonlinear case, which implies that the linearization favors a stronger El Niño event. In other words, the nonlinearity in the wind stress anomaly term suppresses El Niño. For a La Niña event, the wind stress anomaly is negative, that is, an easterly anomaly. The linearization will reduce this easterly anomaly and induce a much weaker La Niña event. In summary, the nonlinearity associated with the wind stress anomaly suppresses El Niño and enhances La Niña, leading to an ENSO asymmetry in which El Niño is weaker than La Niña.

[30] In the second group, we linearized the parameterized subsurface temperature in the ZC model but kept the other nonlinear terms unchanged. It is found that the linearized subsurface temperature term for El Niño is larger than its nonlinear counterpart, namely, the subsurface temperature becomes warmer owing to the linearization. As a result, the temperature of the upwelled water is warmer in the linearized case, which will cause a much stronger El Niño event in comparison to the nonlinear case. That is to say, the nonlinearity related to the subsurface temperature parameterization suppresses El Niño. For a La Niña event, the linearization weakens the subsurface temperature, therefore, favors a stronger La Niña. Equivalently, the nonlinearity

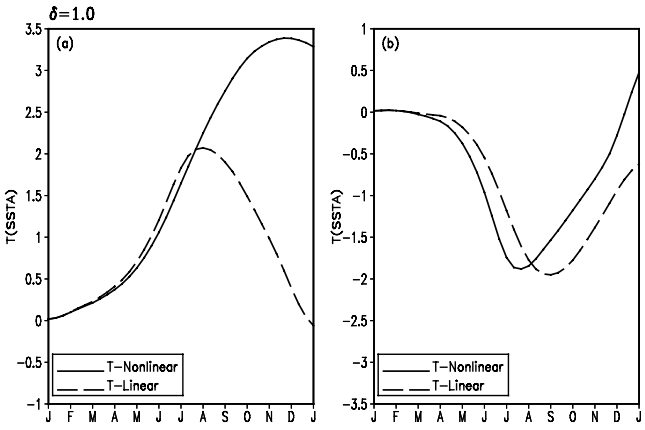

Figure 5. Same as Figure 4 except for $\delta = 1.0$.

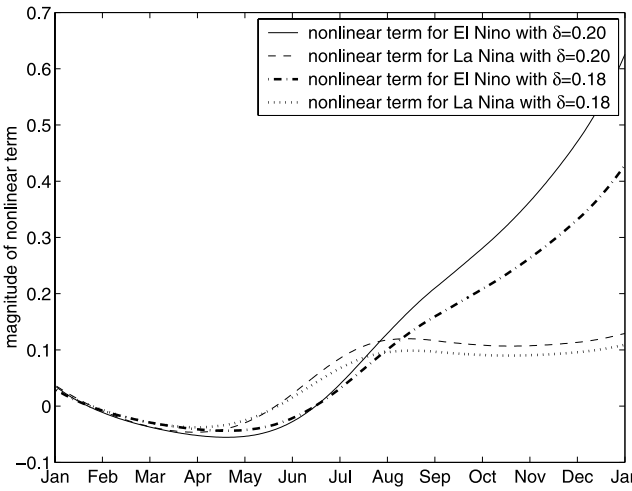

Figure 6. Time-dependent evolution of the NTA in the WF96 model. Solid (dashed) line represents that of the El Niño (La Niña) with $\delta = 0.20$, and dash-dotted (dotted) line denotes that of the El Niño (La Niña) with $\delta = 0.18$.

associated with the subsurface temperature suppresses La Niña. In addition, we found that the amplitude difference between linearized and nonlinear subsurface temperature terms for La Niña is larger than that for El Niño. Though the nonlinearity related to subsurface temperature suppresses both El Niño and La Niña, the extent of the suppression is larger for La Niña than for El Niño, leading to an ENSO asymmetry with stronger El Niño and weaker La Niña. The asymmetry induced by the parameterized subsurface temperature, however, can be counteracted by that caused by the wind stress anomaly; therefore the net effect of the two terms has little impact on the ENSO asymmetry in the ZC model, which also shed lights on the symmetry of the El Niño and La Niña in the PL-ZC model.

[31] These two groups of sensitivity experiments help to trace the origin of the ENSO asymmetry. Among the three kinds of nonlinearities in the ZC model, the effect of the nonlinearity of the subsurface temperature parameterization on ENSO asymmetry can be offset by that of the wind stress anomaly, which leaves the nonlinearity related to the NTA to play the decisive role in ENSO asymmetry. These results of the ZC model support those of the WF96 model. That is, the NTA considerably enhances El Niño and trivially affects La Niña amplitude. Then what is the mechanism? Why do the results of the ZC model support those of the WF96 model?

4. Interpretation of the Role of NTA in ENSO Asymmetry

4.1. Why Does the NTA Aggressively Enhance El Niño and Negligibly Affect La Niña Amplitude?

[32] The asymmetry of El Niño and La Niña in amplitude is an essential characteristic of ENSO. Generally, the physical explanation of fundamental characteristics for ENSO requires a theoretical model [*Wang and Fang*, 1996; *Jin*, 1997a, 1997b; *Wang*, 2001; *Wang et al.*, 1999; *Tziperman et al.*, 1994]. As shown in previous sections, the WF96 model is a theoretical ENSO model and particularly captures the asymmetry of ENSO. Furthermore, its results can be supported by those of the realistic ZC model. Therefore we use the WF96 model to address the mechanism of ENSO asymmetry.

[33] Numerical results shown in section 3 demonstrate that the NTA plays the decisive role in ENSO asymmetry. The NTA is included in temperature equation of the model. In Figure 6, we plot the time-dependent NTA for El Niño and La Niña in the WF96 model. It is illustrated that the magnitude of the NTA for El Niño is very large (particularly in mature phase), but for La Niña it is negligible, although both of them begin to become positive in summer. The temperature equation in the WF96 model suggests that the positive (negative) SSTA during El Niño (La Niña) period positively (negatively) feeds back on the positive NTA. Thus we conclude that the El Niño is considerably enhanced by the large NTA through the nonlinear feedback, while the La Niña is trivially affected by the small NTA.

[34] Figure 6 also suggests that the magnitude of the NTA for the relatively strong El Niño event induced by CNOP with $\delta = 0.20$ is considerably larger than that for the weak El Niño event with $\delta = 0.18$. This suggests that the larger the El Niño amplitude, the larger the magnitude of the NTA. From the temperature equation in the WF96 model, it is understandable that the effect of the NTA on a strong El Niño is larger than that on a weak one. Also, it is clear from Figure 6 why the most considerable asymmetry of ENSO occurs during the mature phase of the El Niño.

[35] Now we explain the mechanism by which the NTA affects the ENSO asymmetry. The NTA, $\eta(T, h) = T(T - \gamma h)$, is related to the anomalous zonal SST gradient and the anomalous vertical temperature gradient (see section 4.2). On the basis of the WF96 model, we plot in Figures 7 and 8 the anomalous temperature difference between equatorial eastern and western Pacific, and between mixed-layer and

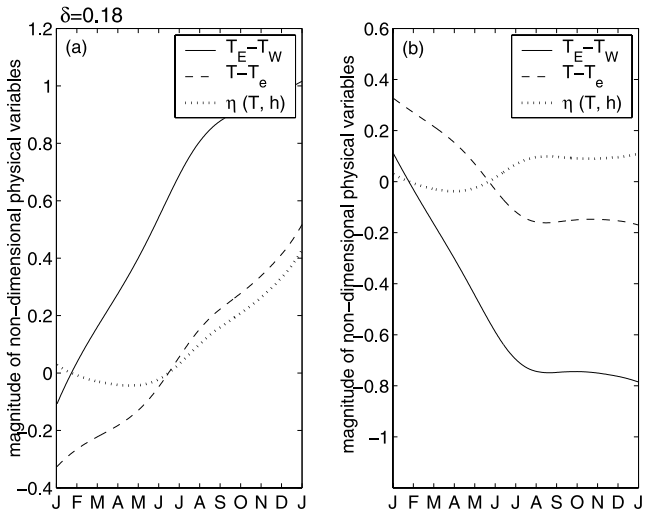

Figure 7. Time-dependent anomalous SST difference between equatorial eastern and western Pacific (solid line), $T_E - T_W$, the anomalous temperature difference between mixed-layer and subsurface-layer water (dashed line), $T - T_e$, and the NTA (dotted line), $\eta(T, h)$. (a) El Niño caused by CNOP with $\delta = 0.18$. (b) La Niña by local CNOP with $\delta = 0.18$.

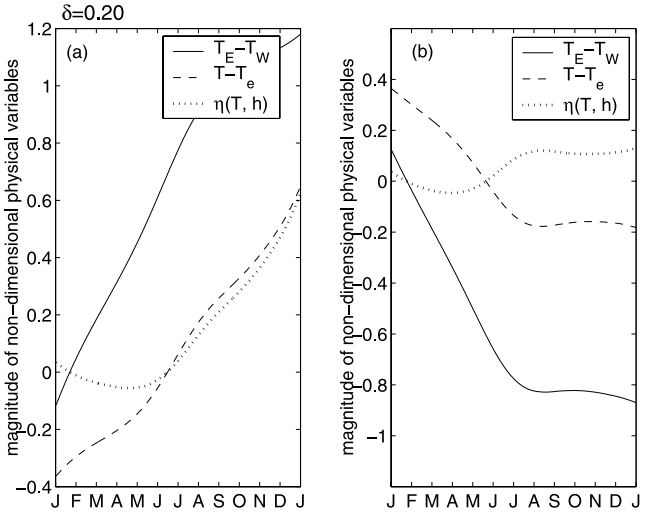

Figure 8. Same as Figure 7 except for $\delta = 0.20$.

subsurface-layer water during El Niño and La Niña periods, respectively. It is demonstrated that both the anomalous zonal SST difference and the vertical temperature difference tend to increase to be positive with the development of El Niño, and the NTA also becomes gradually large (Figures 7a and 8a). In fact, during an El Niño when the SSTA, T, becomes large, the warming in the eastern Pacific increases the zonal SST difference and the anomalous westerly, which weakens the anomalous upwelling, w. The weak anomalous upwelling acts on the increasing anomalous vertical temperature difference, $T - T_e = T - \mu h$ (where T_e denotes the anomalous temperature of the entrained water from beneath the mixed layer [*Wang et al.*, 1999]) and much favors the strengthening of El Niño, which implies that the NTA enhances El Niño. For La Niña events, it is shown that both the anomalous zonal SST difference and vertical temperature difference decrease to be negative with the development of La Niña (Figures 7b and 8b). Physically, the cooling decreases the anomalous vertical temperature difference to be negative, which means that $T < T_e$ with $T < 0$ and $T_e < 0$. That is, the anomalous temperature of the upwelled water is larger than the SSTA. Although the decreasing anomalous zonal SST difference increases the anomalous upwelling, the negative anomalous vertical temperature difference will offset the contribution of the anomalous upwelling to SST cooling and suppresses the La Niña amplitude. It implies that the NTA suppresses the La Niña amplitude. Then why does the NTA have a bigger effect on El Niño than on La Niña?

[36] The amplitudes of both the anomalous zonal SST difference and the anomalous vertical temperature difference for La Niña are much smaller than those for El Niño (Figures 7 and 8). Owing to the small anomalous vertical temperature difference during La Niña, the anomalous temperature of the upwelled water will have a small effect on the contribution of the anomalous upwelling to SST cooling. However, for El Niño, the large anomalous SST difference will remarkably strengthens westerly anomaly, which acts on the large anomalous vertical temperature difference and considerably enhances El Niño. Consequently, the amplitude suppression of La Niña has a much smaller extent than the enhancing of El Niño amplitude.

[37] These above discussions on the mechanism of ENSO asymmetry are based on the simple models. It is expected that they are also true in more complex models. It is also hopeful that the physics for ENSO asymmetry can be further explored with more realistic models.

4.2. Why Do the Results of the ZC Model Support Those of WF96 Model?

[38] The results of the ZC model on ENSO asymmetry support those of the WF96 model, which suggested using the theoretical WF96 model to explain the mechanism of the ENSO asymmetry in section 4.1. Now we turn to analyze why the NTA term in the ZC model has the same role in ENSO asymmetry as that in the highly simplified WF96 model.

[39] The NTA term in the ZC model is

$$\psi(U, w_s) = \boldsymbol{U} \cdot \nabla \boldsymbol{T} - (M(\bar{\boldsymbol{w}}_s + \boldsymbol{w}_s) - M(\bar{\boldsymbol{w}}_s))\boldsymbol{T}_z. \quad (7)$$

The second term in equation (7), denoted by $\varphi(w_s)$, represents the anomalous vertical temperature advection. In the expression of $\varphi(w_s)$, $M(\bar{w}_s)$ describes the mean upwelling that suppresses (enhances) warming (cooling) and is equal to $\bar{w}_s$ (>0), and $M(\bar{w}_s + w_s)$ represents the total upwelling and is equal to either $\bar{w}_s + w_s$ or 0. Consequently, $M(\bar{w}_s + w_s) - M(\bar{w}_s)$ is equal to w_s or $-\bar{w}_s$. For convenience, we write $\varphi(w_s)$ as wT_z, where $w = w_s > 0$ (or $w = -\bar{w}_s < 0$), indicating the anomalous upwelling (or downwelling) that could enhance (or suppress) mean upwelling and induce anomalous cooling (or warming). Thus equation (7) becomes to

$$\psi(U, w) = \boldsymbol{U} \cdot \nabla \boldsymbol{T} - \boldsymbol{w}\boldsymbol{T}_z. \quad (8)$$

In the WF96 model, the meridional temperature advection was negligible. Thus we have

$$\psi(u, w) = \boldsymbol{u}\frac{\partial T}{\partial x} - \boldsymbol{w}\boldsymbol{T}_z, \quad (9)$$

where u is the zonal current. The WF96 demonstrated that u and w can be obtained by the following diagnostic equation:

$$u = -\frac{g'}{\beta y}\frac{\partial h}{\partial y}, \quad (10)$$

$$w = -\frac{(H - H_1)\beta d R}{r_s^2 r_a}\frac{\partial T}{\partial x}, \quad (11)$$

where β is the equatorial planetary vorticity gradient, g' the reduced gravity, d the atmospheric boundary layer depth normalized by the atmospheric density scale, R the gas constant, and r_s and r_a the Rayleigh friction coefficients in the oceanic mixed layer and in the atmospheric boundary layer, respectively. Using equations (10) and (11) into (9) and the given characteristic scales in the WF96 to scale x, y, T, and h, $\psi(u, w_s)$ can be written as follows:

$$\psi(u', w') = C\frac{\partial T'}{\partial x'}\left(T' - \mu h' + \delta_1 \frac{1}{y'}\frac{\partial h'}{\partial y'}\right), \quad (12)$$

where the prime denotes a nondimensional quantity, μ measures the coupling strength between thermocline and SST, δ_1 represents the contribution of the horizontal temperature by anomalous zonal currents to local SST variation, and $C = \frac{\theta\beta g' H_2}{L_x r_s^2}$ is a constant. By using the assumption of the lowest-order parabolic cylindrical function for nondimensional meridional structure in the WF96, equation (12) becomes

$$\psi(u', w') = C' \frac{\partial T'}{\partial x'} [T' - (\mu + \delta_1) h']. \tag{13}$$

[40] In the theoretical WF96 model, ENSO is treated as a basin wide standing mode with one pole in the equatorial eastern Pacific ($x_E = 0.5$ representing 120°W) and the other in the western Pacific ($x_E = -0.5$ representing 160°E). Having considered observations and simplicity, the WF96 assume that the SST anomalies vanish in western Pacific and its amplitude increases eastward linearly. Then $\frac{\partial T}{\partial x} = T_E$, and the anomalous temperature advection in eastern Pacific is reduced to

$$\eta(T_E, h_E) = C' T_E (T_E - \gamma h_E), \tag{14}$$

where $\gamma = \mu + \delta_1$. Equation (14) is the nonlinear term in the WF96 model, which is similar to that in the ZC model, equation (13). This is why the results of the ZC model support those of the WF96 model.

5. Conclusion and Discussion

[41] The theoretical WF96 model and the intermediate ZC model are used to reveal ENSO asymmetry by using the new approach of CNOP. The results demonstrate that the El Niño event caused by the CNOP in the WF96 model is drastically stronger than the La Niña event caused by the local CNOP. The stronger the El Niño event is, the more significant the ENSO asymmetry is. We also explain the essential mechanism of the amplitude asymmetry of the observed ENSO by investigating the evolutions of CNOP and local CNOP in the tangent linear model (TLM), a linearized form of the WF96 model. It is shown that the evolutions of CNOP and local CNOP in the TLM also evolve respectively into an El Niño event and a La Niña event, but they tend to be symmetric in amplitude. Furthermore, the amplitude of the El Niño in the TLM is considerably smaller than that of the El Niño in the WF96 model, while the La Niña events in the WF96 model and its TLM remain similar. These results show that nonlinearity plays an important role in ENSO asymmetry. Similar results are obtained in the ZC model. By analyzing the roles of different nonlinearity terms in the ZC model, we clearly identify the origin of ENSO asymmetry and emphasize the decisive role of NTA in ENSO asymmetry.

[42] On the basis of the WF96 model, we explain why the NTA aggressively enhances El Niño and trivially affects La Niña amplitude. The NTA is closely related to the dynamical behavior of the anomalous temperature difference between equatorial eastern and western Pacific, and between surface-layer and subsurface-layer water. We demonstrate that these two kinds of temperature differences tend to increase (decrease) during El Niño (La Niña), both of which favor positive NTA. However, the amplitudes of the NTA during El Niño and La Niña are significantly different. The NTA for El Niño become aggressively large with the development of El Niño owing to the significant increasing of the above temperature differences, while for La Niña it is always very small during the La Niña event since the decreasing vertical temperature difference offset trivially the contributions of anomalous upwelling to SST cooling. In fact, from these discussions, one can easily see that the asymmetry of the NTA evolutions during El Niño and La Niña results in the ENSO asymmetry.

[43] *Jin et al.* [2003] and *An and Jin* [2004] examined the role of nonlinear dynamical heating in ENSO asymmetry. We demonstrate similar results. Then, we use a new approach to explore the roles of different types of nonlinearities in ENSO asymmetry and emphasize the decisive role of the NTA in ENSO asymmetry. Furthermore, we give a possible physical explanation of ENSO asymmetry based on a theoretical model.

[44] In the observation, it is after 1976 that the strong ENSO has the significant asymmetry in amplitude [*Duan and Mu*, 2006], which can then be regarded as an evidence that ENSO underwent a dynamic shift around 1976 from a relatively stable to an unstable coupled system. Our theoretical results may explain this shift of ENSO: the occurrence of this dynamic shift may result from the change of the NTA on interdecadal scale [*An*, 2004; *Duan and Mu*, 2006].

[45] We also note that in the ZC model the El Niño peaks in late winter, but in the PL-ZC model, the mature phase of the El Niño event tends to lock to boreal Autumn (see Figure 4). It seems that the nonlinearity affects the mature phase of El Niño. Since the phase-locking characteristic of La Niña events cannot be well modeled by the ZC model [*An and Wang*, 2001], no attempt is made in this paper to discuss the effect of nonlinearity on phase-locking of El Niño and La Niña. It is expected that a more complex model will be used to address this issue in the future.

[46] **Acknowledgments.** We thank three anonymous reviewers for their insightful suggestions. We also thank Bin Wang from University of Hawaii for his valuable comments. Thanks are also extended to Zuojun Yu from IPRC for her useful suggestions on an early version of the manuscript. This study has been jointly supported by 973 Program (2006CB403606), KZCX3-SW-230 of the Chinese Academy of Sciences, and the NSFC of China (40523001, 40505013, 40675030).

References

An, S.-I. (2004), Interdecadal changes in the El Niño–La Niña asymmetry, *Geophys. Res. Lett.*, *31*, L23210, doi:10.1029/2004GL021699.

An, S.-I., and F. F. Jin (2000), An eigen analysis of the interdecadal changes in the structure and frequency of ENSO mode, *Geophys. Res. Lett.*, *27*, 2573–2576.

An, S.-I., and F. F. Jin (2004), Nonlinearity and asymmetry of ENSO, *J. Clim.*, *17*, 2399–2412.

An, S.-I., and B. Wang (2001), Mechanisms of locking the El Niño and La Niña mature phases to boreal winter, *J. Clim.*, *14*, 2164–2176.

Birgin, E. G., J. M. Martinez, and M. Raydan (2000), Nonmonotone spectral projected gradient methods on convex sets, *SIAM J. Control Optim.*, *10*, 1196–1211.

Clarke, A. J., and S. Van Gorder (1999), On the connection between the boreal spring southern oscillation persistence barrier and the tropospheric biennial oscillation, *J. Clim.*, *12*, 610–620.

Duan, W. S., and M. Mu (2006), Investigating decadal variability of El Niño–Southern Oscillation asymmetry by conditional nonlinear optimal perturbation, *J. Geophys. Res.*, *111*, C07015, doi:10.1029/2005JC003458.

Duan, W. S., M. Mu, and B. Wang (2004), Conditional nonlinear optimal perturbation as the optimal precursors for El Niño–Southern Oscillation events, *J. Geophys. Res.*, *109*, D23105, doi:10.1029/2004JD004756.

Jin, F. F. (1997a), An equatorial ocean recharge paradigm for ENSO. Part I: Conceptual model, *J. Atmos. Sci.*, *54*, 811–829.

Jin, F. F. (1997b), An equatorial ocean recharge paradigm for ENSO. Part II: A stripped-down coupled model, *J. Atmos. Sci.*, *54*, 830–847.

Jin, F. F., S.-I. An, A. Timmermann, and J. X. Zhao (2003), Strong El Niño events and nonlinear dynamical heating, *Geophys. Res. Lett.*, *30*(3), 1120, doi:10.1029/2002GL016356.

Mu, M., and W. S. Duan (2003), A new approach to studying ENSO predictability: Conditional nonlinear optimal perturbation, *Chin. Sci. Bull.*, *48*, 1045–1047.

Mu, M., and W. S. Duan (2005), Conditional nonlinear optimal perturbation and its applications to the studies of weather and climate predictability, *Chin. Sci. Bull.*, *50*, 2401–2407.

Mu, M., and Z. Y. Zhang (2006), Conditonal nonlinear optimal perturbation of a barptrophic model, *J. Atmos. Sci.*, *63*, 1587–1604.

Mu, M., W. S. Duan, and B. Wang (2003), Conditional nonlinear optimal perturbation and its applications, *Nonlinear Processes Geophys.*, *10*, 493–501.

Mu, M., L. Sun, and D. A. Henk (2004), The sensitivity and stability of the ocean's thermocline circulation to finite amplitude freshwater perturbations, *J. Phys. Oceanogr.*, *34*, 2305–2315.

Münnich, M., M. A. Cane, and S. E. Zebiak (1991), A study of self-excited oscillations of the tropical ocean-atmosphere system. Part II: Nonlinear cases, *J. Atmos. Sci.*, *48*, 1238–1248.

Peland, C., and P. Sardeshmukh (1995), The optimal growth of tropical sea surface temperature anomalies, *J. Clim.*, *8*, 1999–2004.

Philander, S. G. H. (1983), El Niño Southern Oscillation phenomena, *Nature*, *302*, 295.

Rodgers, K. B., P. Friederichs, and M. Latif (2005), Tropical Pacific decadal variability and its relation to decadal modulations of ENSO, *J. Clim.*, *17*, 3761–3774.

Sun, L., M. Mu, D. J. Sun, and X. Y. Yin (2005), Passive mechanism of decadal variation of thermohaline circulation, *J. Geophys. Res.*, *110*, C07025, doi:10.1029/2005JC002897.

Timmermann, A., and F. F. Jin (2002), A nonlinear mechanism for decadal El Niño amplitude changes, *Geophys. Res. Lett.*, *29*(1), 1003, doi:10.1029/2001GL013369.

Tziperman, E., L. Stone, M. A. Cane, and H. Jarosh (1994), El Niño Chaos: Overlapping of resonances between the seasonal cycle and the Pacific Ocean-Atmosphere oscillator, *Science*, *264*, 72–74.

Wang, B., and S.-I. An (2001), Why the properties of El Niño changed during the late 1970s, *Geophys. Res. Lett.*, *28*, 3709–3712.

Wang, B., and Z. Fang (1996), Chaotic oscillation of tropical climate: A dynamic system theory for ENSO, *J. Atmos. Sci.*, *53*, 2786–2802.

Wang, B., A. Barcilon, and Z. Fang (1999), Stochastic dynamics of El Niño–Southern Oscillation, *J. Atmos. Sci.*, *56*, 5–23.

Wang, C. (2001), A unified oscillator model for the El Niño–Southern Oscillation, *J. Clim.*, *24*, 98–115.

Wang, C., and J. Picaut (2004), Understanding ENSO physics—A review, in *Earth's Climate: The Ocean-Atmosphere Interaction*, *Geophys. Monogr. Ser.*, vol. 147, edited by C. Wang, S.-P. Xie, and J. A. Carton, pp. 21–48, AGU, Washington, D. C.

Wilcoxon, F. (1945), Individual comparisons by ranking methods, *Biometrics*, *1*, 80–83.

Zebiak, S. E., and A. Cane (1987), A model El Niño–Southern Oscillation, *Mon. Weather Rev.*, *115*, 2262–2278.

W. Duan, M. Mu, and H. Xu, LASG, Institute of Atmospheric Physics, Chinese Academy of Sciences, Beijing 100029, China. (duanws@lasg.iap.ac.cn)